Electrically Tunable Single Polaritonic Quantum Dot at Room Temperature

Hyeongwoo Lee,[1] Benjamin G. Whetten,[2] Byong Jae Kim,[3] Ju Young Woo,[4] Yeonjeong Koo,[1] Jinhyuk Bae,[1] Mingu Kang,[1] Taeyoung Moon,[1] Huitae Joo,[1] Sohee Jeong,[3,5] Jaehoon Lim,[3,5] Alexander L. Efros,[6] Markus B. Raschke,[2,*] Matthew Pelton,[7,†] and Kyoung-Duck Park[1,‡]

[1]*Department of Physics, Pohang University of Science and Technology (POSTECH), Pohang 37673, Republic of Korea*
[2]*Department of Physics and JILA, University of Colorado, Boulder, Colorado 80309, USA*
[3]*Department of Energy Science, Center for Artificial Atoms, Sungkyunkwan University (SKKU), Suwon 16419, Republic of Korea*
[4]*Digital Transformation R&D Department, Korea Institute of Industrial Technology (KITECH), Ansan 15588, South Korea*
[5]*SKKU Institute of Energy Science and Technology (SIEST), Sungkyunkwan University, Suwon 16419, Republic of Korea*
[6]*Naval Research Laboratory, Washington, DC 20375, USA*
[7]*Department of Physics, University of Maryland, Baltimore County (UMBC), Baltimore, Maryland 21250, USA*

(Received 7 December 2023; accepted 28 February 2024; published 25 March 2024)

Exciton-polaritons confined in plasmonic cavities are hybridized light-matter quasiparticles, with distinct optical characteristics compared to plasmons and excitons alone. Here, we demonstrate the electric tunability of a single polaritonic quantum dot operating at room temperature in electric-field tip-enhanced strong coupling spectroscopy. For a single quantum dot in the nanoplasmonic tip cavity with variable dc local electric field, we dynamically control the Rabi frequency with the corresponding polariton emission, crossing weak to strong coupling. We model the observed behaviors based on the quantum confined Stark effect in the strong coupling regime.

DOI: 10.1103/PhysRevLett.132.133001

Two-level emitters coupled to an optical cavity exhibit modified spontaneous emission behaviors depending on the interaction with the surrounding density of states [1]. In contrast to the weak coupling regime where the emitters exhibit Purcell-enhanced spontaneous emission [2,3], the emitter coupled to the cavity with its coupling strength g exceeding the emitter decay rate (γ) and cavity loss rate (κ) forms the quantum hybridized state of light and matter, with the coherent energy exchange between the emitter and the cavity. It gives rise to the Rabi splitting in the optical responses, e.g., scattering or photoluminescence (PL) spectrum [4–8]. In this strongly coupled system, manipulation of the quantum hybridized states induces a variety of quantum optical responses, leading to a broad range of applications in quantum optical devices [9–12].

In dielectric cavities, the diffraction-limited mode volume requires high quality (Q) factors and low temperature to achieve strong coupling, following $\kappa \propto Q^{-1}$ and $\gamma \propto k_B T$, respectively [13–15]. The high Q cavities result in the narrow spectral overlap between the emitter and the cavity, i.e., narrow on-resonance condition, for maintaining strong coupling. These constraints significantly compromise the controllability of the quantum hybridized states, consequently limiting the investigation of the quantum electrodynamic phenomena in the strong coupling regime. Recently, the platform of plasmonic cavities achieved effective strong coupling between plasmons and excitons, even at room temperature owing to its nanoscale mode volume [5,7,16]. The nanoscale mode volume of the plasmonic cavities significantly enhances the coupling strength and consequently facilitates the strong coupling with low Q system, significantly increasing the tuning range of the coupling strength. Therefore, in contrast to the electrical control of the single quantum dot (QD) strongly coupled to photonic crystal cavities [15,17,18], exhibiting detuning-sensitive polariton emission [19], the expanded spectral bandwidth of the plasmonic system provides a platform to directly modify the coupling strength. While these advantages can lead us to investigate and control quantum electrodynamic phenomena in the strong coupling regime for realizing practical quantum optoelectronic devices [20], the electrical tunability of polaritonic states has not been demonstrated in a plasmonic cavity system or at room temperature.

Here, we present an electrically tunable single polaritonic QD at room temperature, operating with the newly developed electric-field tip-enhanced strong coupling (e-TESC) spectroscopy. In e-TESC, we dynamically control the polariton PL energy by exploiting the quantum confined Stark effect (QCSE). In contrast to a single QD in a dielectric cavity, by exploiting the broad range of spectral overlap between the emitter and cavity resonance at room temperature, we show the wide tunability of the coupling strength up to ~80 meV, crossing between the weak and strong coupling regime. In addition, for different single QDs within the same cavity, we observe the differentiated responses of the polariton emission under the control of the external electric field, confirming the differently oriented

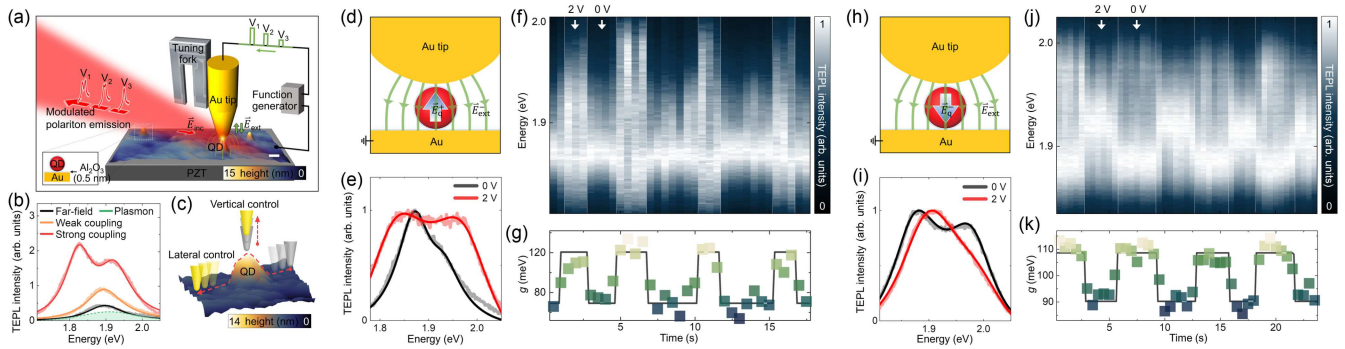

FIG. 1. *e*-TESC spectroscopy and electrical control of polaritonic states. (a) Illustration of *e*-TESC spectroscopy. Under optical excitation $\vec{E}_{\mathrm{inc}}$, single isolated QD confined to nanoplasmonic tip-cavity can reach strong coupling regime and generates polariton emission even at room temperature. Inducing tip-sample bias results in localized external electric field $\vec{E}_{\mathrm{ext}}$ to strongly coupled QD in tip cavity, modifying polaritonic states. Scale bar is 50 nm. (b) PL spectra of single QD uncoupled (black, without tip), weakly coupled (orange, tip-QD distance ~10 nm), and strongly coupled (red, tip-QD distance <3 nm) to tip-cavity induced plasmon (green). The PL spectrum of tip-cavity induced plasmon is independently measured without the QD. (c) Topography image of single isolated QD and illustration of three-dimensional plasmonic tip control. Scale bar is 50 nm. (d) Illustration of single isolated QD with upward built-in electric field $\vec{E}_{\mathrm{q}}^{+}$. (e) TEPL spectra with (red) and without (black) downward external electric field $\vec{E}_{\mathrm{ext}}^{-}$. In this case, the external electric field is applied in the opposite direction. Dynamic electrical switching of polariton emission (f) and corresponding coupling strength (g). (h) Illustration of a single isolated QD with downward built-in electric field $\vec{E}_{\mathrm{q}}^{-}$. (i) TEPL spectra with (red) and without (black) downward external electric field $\vec{E}_{\mathrm{ext}}^{-}$. Dynamic electrical switching of polariton emission (j) and corresponding coupling strength (k).

built-in dipole moment of QDs and its effect on the polariton energy modulation. These experimental results of electrically tunable strong coupling system are quantitatively analyzed with the extended theoretical model of QCSE in the strong coupling regime.

Figure 1(a) illustrates the experimental setup used to demonstrate *e*-TESC (see Supplemental Material, S1 [21]). A conductive Au tip on the template stripped Au surface forms the nanocavity with local electric field control (Supplemental Material, Fig. S2 [21]). For the quantum emitter, we spin coat $CdSe/Zn_{1-x}Cd_xS$ QDs on the Au surface with Al_2O_3 capping layer of 0.5 nm thickness to prevent a photooxidation under ambient conditions (Supplemental Material, Figs. S3–S6 [21]). By employing a shear-force AFM technique, we regulate the cavity gap with <0.1 nm precision (Supplemental Material, Fig. S7 [21]). Photoluminescence spectra are measured for single QDs within the plasmonic nanocavity to characterize the QD-cavity coupling. With the tip placed immediately above a single QD, the coupling between the QD and the tip-cavity plasmon can reach the strong coupling regime, generating polariton emission, as shown in Fig. 1(b) (Supplemental Material, Figs. S8 and S9 [21]). Three-dimensional control of the plasmonic tip position enables the coupling strength to be optimized, as illustrated in Fig. 1(c) (Supplemental Material, Fig. S10 [21]) [7].

The majority of the measured QDs exhibit negligible or irregular changes in their PL spectrum when an external field is applied across the tip-substrate gap. For a small fraction of the QDs, we observe systematic and reversible changes in the PL spectra under applied external field $\vec{E}_{\mathrm{ext}}^{-}$. This is attributed to the sensitivity of the coupling strength with respect to the dipole orientation of QDs given by $g = \sqrt{\hbar\omega_c|\varepsilon\cdot\mu|^2/2\varepsilon_0 V_m}$, where $\hbar$, ω_c, ε, μ, ε_0, and V_{m} denote the reduced Planck's constant, resonance frequency of the cavity field, polarization unit vector along the polarization axis of the cavity plasmon, transition dipole moment of the emitter, vacuum permittivity, and cavity mode volume, respectively (Supplemental Material, Fig. S11 [21]). As a result, two distinct examples are illustrated in Figs. 1(d)–1(k): an increase or a decrease in the QD-cavity coupling strength under a positive applied bias (Supplemental Material, Fig. S12 [21]). To quantify the change in coupling strength g under applied bias, we fit the experimentally obtained tip-enhanced photoluminescence (TEPL) spectra to a coupled harmonic oscillator model [7]:

$$I_{\mathrm{PL}}(\omega) = \frac{\gamma_{\mathrm{QD}}}{2\pi}\left|\frac{\gamma_{\mathrm{SP}}/2 - i(\omega-\omega_{\mathrm{SP}})}{\{(\gamma_{\mathrm{SP}}+\gamma_{\mathrm{QD}})/4 - i(\omega_{\mathrm{QD}}-\omega_{\mathrm{SP}})/2 - i(\omega-\omega_{\mathrm{QD}})\}^2+\Omega^2}\right|^2, \quad (1)$$

TABLE I. Parameters for fitting TEPL spectra with different external electric bias.

	Fig. 1(f)		Fig. 1(j)	
	Bias = 0 V	Bias = 2 V	Bias = 0 V	Bias = 2 V
ω_{QD} (eV)	1.879	1.890	1.920	1.918
ω_{SP} (eV)	1.900	1.900	1.935	1.935
γ_{QD} (eV)	0.090	0.090	0.090	0.090
γ_{SP} (eV)	0.195	0.195	0.180	0.180
g (eV)	0.076	0.116	0.108	0.091

$$\Omega = \frac{1}{2}\sqrt{g^2 + (\omega_{QD} - \omega_{SP}) - \frac{(\gamma_{SP} - \gamma_{QD})^2}{4}}, \qquad (2)$$

where Ω, ω_{QD}, ω_{SP}, γ_{QD}, and γ_{SP} denote vacuum Rabi frequency, the resonance frequency of QD, the resonance frequency of plasmon, the decay rate of QD, and the decay rate of plasmon, respectively. For a given QD, ω_{SP} and γ_{SP} are independent of the applied field, as the tip position is rigidly fixed during the electric field modulation to ensure the fixed cavity mode volume (see Supplemental Material, Figs. S13–S15 [21]). Table I shows the average fitting parameters to generate the fits of TEPL spectra in Figs. 1(f) and 1(j). For an applied bias of +2 V, g changes by +80 meV for the first QD and −29 meV for the second QD. Here, we neglect any potential additional dephasing due to the applied electric fields, which is expected to be small compared to the thermal contributions to dephasing of colloidal QDs at room temperature [39]. We tentatively attribute the different sign of the change in g to built-in electric fields, or dipole moments, in the QDs [see Figs. 1(d) and 1(h)]. These dipole moments either oppose to add to the applied bias, leading to the different observed responses.

To systematically investigate the role of built-in electric field of QD in e-TESC experiments, we measured the photoluminescence spectra as a function of the applied field. Results are shown for three specific QDs in Fig. 2. These QDs illustrate the three types of behavior that were observed. In Figs. 2(a) and 2(b), the Rabi splitting quadratically decreases for both positive and negative applied bias. This can be attributed to a QD with no built-in electric field, or whose dipole moment is perpendicular to the external electric field. In Figs. 2(c) and 2(d), the Rabi splitting decreases with positive external field and increases with negative external field, corresponding to a QD with upward built-in electric field $\vec{E}_q^+$. Last, in Figs. 2(e) and 2(f), the Rabi splitting increases with positive external electric field and decreases with negative field, corresponding to a QD with downward built-in electric field. These results suggest that a different built-in electric field in QDs leads to a wide range of tunability of coupled QD-nanocavity states, crossing the weak and strong coupling regimes.

The observed results appear to be consistent with tuning of the QD transition energy and dipole moment through the QCSE (see Supplemental Material, Figs. S16 and S17 [21]). In the QCSE, an external electric field tilts the band edges, leading to a quadratic shift in the confined energy levels. The result is a quadratic decrease in the optical transition frequency ω_{QD}, analogous to the Stark effect in atoms.

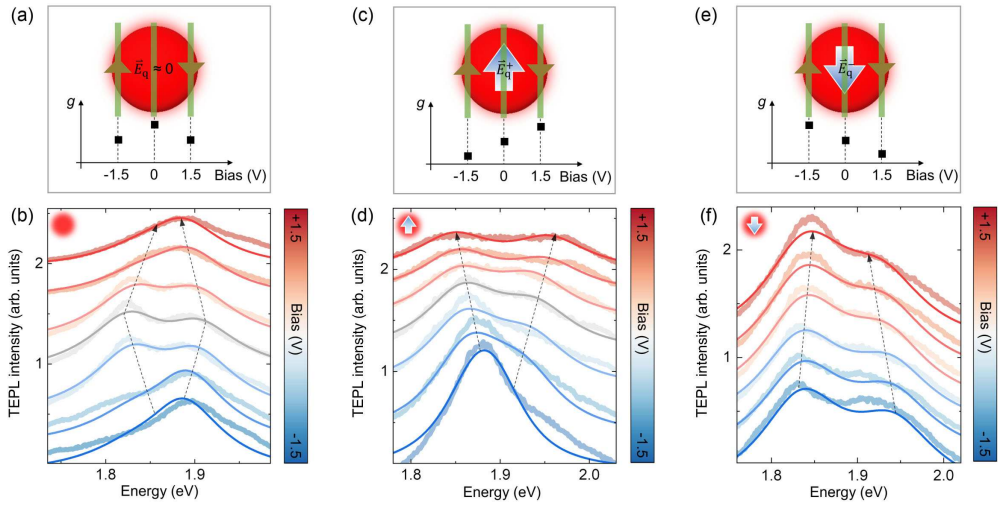

FIG. 2. Polariton emission of single QDs with different built-in electric fields. Illustration of coupling strength g as a function of external electric bias for $\vec{E}_q \approx 0$ (a), upward $\vec{E}_q^+$ (c), and downward $\vec{E}_q^-$ (e) built-in electric fields. Experimental TEPL spectra as continuously increasing external electric bias from −1.5 V to 1.5 V for $\vec{E}_q \approx 0$ (b), upward $\vec{E}_q^+$ (d), and downward $\vec{E}_q^-$ (f) built-in electric fields. Strongly coupled TEPL spectra are fitted to coupled harmonic oscillator model (solid line) to clearly present tendency as a function of external electric field.

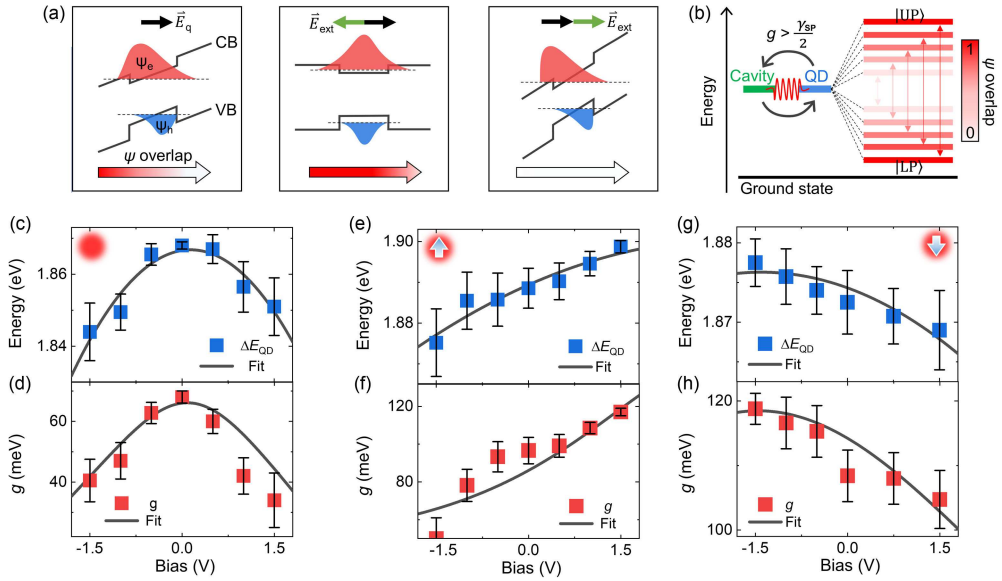

FIG. 3. Quantitative analysis of electrically tunable polaritonic states. (a) Band diagram of QD and corresponding wave function overlap with existence of built-in electric field $\vec{E}_q$ in QD. Depending on the direction of $\vec{E}_{ext}$ with respect to $\vec{E}_q$, spatial distributions of electron and hole wave function can be bidirectionally modulated. (b) Rabi splitting and corresponding coupling strength with changing wave function overlap. Polaritonic parameters (QD energy and g) as function of external electric field for zero (c),(d), upward (e),(f), and downward (g),(h) built-in electric fields, derived from TEPL spectra in Fig. 2. Stark shifts (c),(e),(g) and coupling strengths (d),(f),(h) are quantitatively compared with theoretical model (black line).

Changing ω_{QD} changes the QD-cavity detuning, and thus the coupling strength g, following Eq. (2).

At the same time, the electron and hole wave functions are displaced to opposite sides of the QD [see Fig. 3(a)], decreasing their overlap. This results in a decrease in the transition dipole moment μ, and thus a decrease in the vacuum Rabi frequency Ω, since $\Omega \propto \mu$. The change in Ω, in turn, changes g, again following Eq. (2). The observed changes in g with applied external field can thus be interpreted as being due the combined effects of changing QD-cavity detuning and transition dipole moment.

To quantify these effects, we first fit the observed QD transition frequency ω_{QD} to a quadratic function of the external electric field $\vec{E}_{ext}$ (see Supplemental Material, S18 [21]):

$$\omega_{QD} = -\alpha \cdot (\vec{E}_{ext} - \vec{E}_q)^2 + \omega_{QD_0}, \tag{3}$$

where α is the electrical polarizability, $\vec{E}_q$ is the component of the electric field due to trapped charges q parallel with respect to the applied field, and ω_{QD_0} is the QD transition frequency in the absence of the built-in dipole or external field. Here, we take the total field to be the sum of the external field $\vec{E}_{ext}$ and the built-in electric field $\vec{E}_q$ [40–42]. Figures 3(c), 3(e), and 3(g) show fitting results for the data sets in Fig. 2, and fitting parameters are summarized in Table II. In order to relate these fits of ω_{QD} to the measured changes in g, we develop a simplified analytical model of the QCSE in a spherical core-shell nanocrystal [43–46]. See Supplemental Material, Sec. S17 for details of the model [21]. The result of this model is that

$$g = 2\sqrt{\left(\frac{\Omega_0}{1+\left(\frac{\vec{E}_{ext}-\vec{E}_q}{\Delta E_h^{PS}}\right)^2}\right)^2 - \frac{(\omega_0+\alpha\cdot(\vec{E}_{ext}-\vec{E}_q)^2)^2}{4} + \gamma_0^2}, \tag{4}$$

where Ω_0 is the vacuum Rabi frequency in the absence of either the built-in dipole or external field, $\omega_0 = \omega_{QD} - \omega_{SP}$, $\gamma_0^2 = (\gamma_{SP} - \gamma_{QD})^2/16$, and ΔE_h^{PS} is the difference between the energies of the P and S hole wave functions in the QD.

Since α, $\vec{E}_q$, and ω_{QD_0} are determined by the fit of ω_{QD} as a function of applied field, the only additional fitting parameters for the measured values of g are Ω_0 and ΔE_h^{PS}. Fitting results are shown in Figs. 3(d), 3(f), 3(h), and fitting parameters are summarized in Table II. Specifically, as we fit the data as a function of applied bias V_{ext}, which serves as the actual control parameter in the experiment, the parameters in Eq. (4) are correspondingly represented in the form of built-in bias V_q (V), α' (eV/V^2), and ΔV_h^{PS} (V). The results summarize the three contrasting cases: $\vec{E}_q \approx 0$ [Fig. 2(b)], $\vec{E}_q^+$ [Fig. 2(d)], and $\vec{E}_q^-$ [Fig. 2(f)]. The signs of obtained V_q clearly demonstrate the

TABLE II. Parameters for fitting TEPL spectra with different built-in electric field.

	Figs. 3(c) and 3(d) $\vec{E}_q \approx 0$	Figs. 3(e) and 3(f) $\vec{E}_q^+$	Figs. 3(g) and 3(h) $\vec{E}_q^-$
α' (eV/V^2)	0.009	0.001	0.001
V_q (V)	0.100	3.330	−1.405
ω_{QD_0} (eV)	1.870	1.901	1.876
Ω_0 (eV)	0.033	0.070	0.055
ΔV_h^{PS} (V)	2.200	3.500	6.980

role of built-in electric field $\vec{E}_q$ in bidirectionally controlling polariton emission.

The fitted QD resonances ω_{QD_0} are consistent with the experimentally observed range in Supplemental Material, Fig. S8 (∼1.87–1.92 eV) and vacuum Rabi frequencies Ω_0 are consistent with, albeit somewhat lower than, previously measured values (∼0.05–0.14 eV) [7]. Also, as expected, ΔV_h^{PS} values are larger when α' is lower, since both would result from smaller QD core diameters. However, fitted values of ΔV_h^{PS} are larger than expected. Moreover, the fitted polarizability α is in line with expected values from our model (∼0.002–0.010 eV/V^2) in the case of $\vec{E}_q \approx 0$, but is smaller than expected for the other two cases (Supplemental Material, Fig. S19 [21]). This may be attributed to the limitation of our model assuming Lorentzian line shapes for both the cavity and QD emission. In addition, uncertainties arise from the background gold luminescence and mechanical instabilities under ambient conditions.

The built-in electric field can be attributed to localized charges trapped on the surfaces of the QDs [40,47]. Based on the fitted α, we can estimate the number of charges on the QD surface to generate the fitted V_q of ∼3.330 V and ∼ − 1.405 V, which corresponds to the built-in electric field of ∼0.83 MV/cm and ∼ − 0.35 MV/cm, respectively (Supplemental Material, Sec. S18 [21]). The values of V_q of ∼3.330 V and ∼ − 1.405 V would correspond to trapped surface charges q of ∼1.76e and ∼0.72e, respectively. This is consistent with previous studies indicating that QDs commonly have single, long-lived charges trapped on their surfaces [40]. It indicates that only a small number of charges is sufficient to generate the internal field by the built-in electric field, enabling dynamic electrical control of polariton emission (Supplemental Material, Fig. S20 [21]).

As demonstrated in Eq. (4), the polariton emission under the external electric field can be largely affected by the QD-cavity detuning and the transition dipole moment. At low temperatures, the narrow QD resonances and high cavity Q factors particularly limit the electrical control of the transition dipole moment [15,17,18]. By contrast, the polariton emission at room temperature has less sensitivity to QD-cavity detuning from their wide spectral overlap, indicating the enhanced control range of the transition dipole moment to directly modify the coupling strength in the strong coupling regime. As a result, the polariton energies do not simply follow an single anticrossing curve (Supplemental Material, Fig. S21 [21]), which provides a rigid platform to explore cavity quantum electrodynamics in the strong coupling regime while significantly enhancing the controllability of strongly coupled emission. We find three contrasting polariton emission behaviors upon changing external electric field, realizing the practical control of polaritonic states at room temperature including dynamic switching and bidirectional modulation of the coupling strength with the wide tunable range reaching ∼80 meV.

See Supplemental Material for detailed data, experimental methods, and theoretical model [21].

This work was supported by the National Research Foundation of Korea (NRF) (Grant No. 2020R1C1C1011301) and the Samsung Science and Technology Foundation (Grant No. SSTP-BA2102-05). M. P. acknowledges funding from the Air Force Office of Scientific Research (AFOST Grant No. FA9550-21-1-0272). B. G. H. and M. B. R. acknowledge funding from the National Science Foundation (NSF Grant No. CHE2108009). J. L. and S. J. acknowledge the Creative Materials Discovery Program through the National Research Foundation of Korea (NRF) funded by the Ministry of Science and ICT (No. NRF-2019M3D1A1078299). A. L. E. acknowledges the support of the Office of Naval Research.

*Corresponding author: markus.raschke@colorado.edu
†Corresponding author: mpelton@umbc.edu
‡Corresponding author: parklab@postech.ac.kr

[1] E. M. Purcell, Spontaneous emission probabilities at radio frequencies, Phys. Rev. **69**, 681 (1946).
[2] A. Badolato, K. Hennessy, M. Atature, J. Dreiser, E. Hu, P. M. Petroff, and A. Imamoglu, Deterministic coupling of single quantum dots to single nanocavity modes, Science **308**, 1158 (2005).
[3] D. Englund, D. Fattal, E. Waks, G. Solomon, B. Zhang, T. Nakaoka, Y. Arakawa, Y. Yamamoto, and J. Vučković, Controlling the spontaneous emission rate of single quantum dots in a two-dimensional photonic crystal, Phys. Rev. Lett. **95**, 013904 (2005).
[4] K. Santhosh, O. Bitton, L. Chuntonov, and G. Haran, Vacuum Rabi splitting in a plasmonic cavity at the single quantum emitter limit, Nat. Commun. **7**, ncomms11823 (2016).
[5] H. Groß, J. M. Hamm, T. Tufarelli, O. Hess, and B. Hecht, Near-field strong coupling of single quantum dots, Sci. Adv. **4**, eaar4906 (2018).
[6] H. Leng, B. Szychowski, M.-C. Daniel, and M. Pelton, Strong coupling and induced transparency at room temperature with single quantum dots and gap plasmons, Nat. Commun. **9**, 4012 (2018).

[7] K.-D. Park, M. A. May, H. Leng, J. Wang, J. A. Kropp, T. Gougousi, M. Pelton, and M. B. Raschke, Tip-enhanced strong coupling spectroscopy, imaging, and control of a single quantum emitter, Sci. Adv. **5**, eaav5931 (2019).
[8] Y. Niu, H. Xu, and H. Wei, Unified scattering and photoluminescence spectra for strong plasmon-exciton coupling, Phys. Rev. Lett. **128**, 167402 (2022).
[9] M. S. Tame, K. McEnery, Ş. Özdemir, J. Lee, S. A. Maier, and M. Kim, Quantum plasmonics, Nat. Phys. **9**, 329 (2013).
[10] D. Sanvitto and S. Kéna-Cohen, The road towards polaritonic devices, Nat. Mater. **15**, 1061 (2016).
[11] C. Schneider, A. Rahimi-Iman, N. Y. Kim, J. Fischer, I. G. Savenko, M. Amthor, M. Lermer, A. Wolf, L. Worschech, V. D. Kulakovskii *et al.*, An electrically pumped polariton laser, Nature (London) **497**, 348 (2013).
[12] A. Reiserer, N. Kalb, G. Rempe, and S. Ritter, A quantum gate between a flying optical photon and a single trapped atom, Nature (London) **508**, 237 (2014).
[13] T. Yoshie, A. Scherer, J. Hendrickson, G. Khitrova, H. Gibbs, G. Rupper, C. Ell, O. Shchekin, and D. Deppe, Vacuum Rabi splitting with a single quantum dot in a photonic crystal nanocavity, Nature (London) **432**, 200 (2004).
[14] J. P. Reithmaier, G. Sek, A. Loffler, C. Hofmann, S. Kuhn, S. Reitzenstein, L. Keldysh, V. Kulakovskii, T. Reinecke, and A. Forchel, Strong coupling in a single quantum dot–semiconductor microcavity system, Nature (London) **432**, 197 (2004).
[15] D. Najer, I. Söllner, P. Sekatski, V. Dolique, M. C. Löbl, D. Riedel, R. Schott, S. Starosielec, S. R. Valentin, A. D. Wieck *et al.*, A gated quantum dot strongly coupled to an optical microcavity, Nature (London) **575**, 622 (2019).
[16] R. Chikkaraddy, B. De Nijs, F. Benz, S. J. Barrow, O. A. Scherman, E. Rosta, A. Demetriadou, P. Fox, O. Hess, and J. J. Baumberg, Single-molecule strong coupling at room temperature in plasmonic nanocavities, Nature (London) **535**, 127 (2016).
[17] A. Faraon, A. Majumdar, H. Kim, P. Petroff, and J. Vučković, Fast electrical control of a quantum dot strongly coupled to a photonic-crystal cavity, Phys. Rev. Lett. **104**, 047402 (2010).
[18] A. Laucht, F. Hofbauer, N. Hauke, J. Angele, S. Stobbe, M. Kaniber, G. Böhm, P. Lodahl, M. Amann, and J. Finley, Electrical control of spontaneous emission and strong coupling for a single quantum dot, New J. Phys. **11**, 023034 (2009).
[19] D. A. B. Miller, D. S. Chemla, T. C. Damen, A. C. Gossard, W. Wiegmann, T. H. Wood, and C. A. Burrus, Band-edge electroabsorption in quantum well structures: The quantum-confined Stark effect, Phys. Rev. Lett. **53**, 2173 (1984).
[20] A. F. Kockum, A. Miranowicz, S. De Liberato, S. Savasta, and F. Nori, Ultrastrong coupling between light and matter, Nat. Rev. Phys. **1**, 19 (2019).
[21] See Supplemental Material at http://link.aps.org/supplemental/10.1103/PhysRevLett.132.133001 for detailed data, experimental methods, and theoretical model, which includes Refs. [22–38].
[22] K.-D. Park, M. A. May, H. Leng, J. Wang, J. A. Kropp, T. Gougousi, M. Pelton, and M. B. Raschke, Tip-enhanced strong coupling spectroscopy, imaging, and control of a single quantum emitter, Sci. Adv. **5**, eaav5931 (2019).
[23] M. Flatté, A. Kornyshev, and M. Urbakh, Giant Stark effect in quantum dots at liquid/liquid interfaces: A new option for tunable optical filters, Proc. Natl. Acad. Sci. U.S.A. **105**, 18212 (2008).
[24] J. Li, L. Zhang, and S. Ducharme, Electric energy density of dielectric nanocomposites, Appl. Phys. Lett. **90**, 132901 (2007).
[25] A. Bouhelier, R. Bachelot, G. Lerondel, S. Kostcheev, P. Royer, and G. P. Wiederrecht, Surface plasmon characteristics of tunable photoluminescence in single gold nanorods, Phys. Rev. Lett. **95**, 267405 (2005).
[26] A. Mooradian, Photoluminescence of metals, Phys. Rev. Lett. **22**, 185 (1969).
[27] M. B. Mohamed, V. Volkov, S. Link, and M. A. El-Sayed, The lightning gold nanorods: Fluorescence enhancement of over a million compared to the gold metal, Chem. Phys. Lett. **317**, 517 (2000).
[28] V. Kravtsov, S. Berweger, J. M. Atkin, and M. B. Raschke, Control of plasmon emission and dynamics at the transition from classical to quantum coupling, Nano Lett. **14**, 5270 (2014).
[29] A. Ekinov, A. L. Efros, T. Shubina, and A. Skvortsov, Quantum-size Stark effect in semiconductor microcrystals, J. Lumin. **46**, 97 (1990).
[30] A. L. Efros, M. Rosen, M. Kuno, M. Nirmal, D. J. Norris, and M. Bawendi, Band-edge exciton in quantum dots of semiconductors with a degenerate valence band: Dark and bright exciton states, Phys. Rev. B **54**, 4843 (1996).
[31] V. I. Klimov, *Semiconductor and Metal Nanocrystals: Synthesis and Electronic and Optical Properties* (CRC Press, Boca Raton, 2003).
[32] P. C. Sercel and A. L. Efros, Band-edge exciton in CdSe and other II–VI and III–V compound semiconductor nanocrystals- revisited, Nano Lett. **18**, 4061 (2018).
[33] A. L. Efros and A. L. Efros, Interband absorption of light in a semiconductor sphere, Sov. Phys. Semicond. **16**, 772 (1982).
[34] A. I. Ekimov, F. Hache, M. Schanne-Klein, D. Ricard, C. Flytzanis, I. Kudryavtsev, T. Yazeva, A. Rodina, and A. L. Efros, Absorption and intensity-dependent photoluminescence measurements on CdSe quantum dots: Assignment of the first electronic transitions, J. Opt. Soc. Am. B **10**, 100 (1993).
[35] G. Grigoryan, A. Rodina, and A. L. Efros, Excitons and biexcitons in quantum-well semiconductor microcrystals dispersed in an insulating glassy matrix, Sov. Phys. Solid State **32**, 2037 (1990).
[36] G. W. Wen, J. Y. Lin, H. X. Jiang, and Z. Chen, Quantum-confined Stark effects in semiconductor quantum dots, Phys. Rev. B **52**, 5913 (1995).
[37] Y. Chen, J. Vela, H. Htoon, J. L. Casson, D. J. Werder, D. A. Bussian, V. I. Klimov, and J. A. Hollingsworth, "Giant" multishell CdSe nanocrystal quantum dots with suppressed blinking, J. Am. Chem. Soc. **130**, 5026 (2008).
[38] J. Lim, B. G. Jeong, M. Park, J. K. Kim, J. M. Pietryga, Y.-S. Park, V. I. Klimov, C. Lee, D. C. Lee, and W. K. Bae, Influence of shell thickness on the performance of light-emitting devices based on CdSe/$Zn_{1-x}Cd_x$s core/shell

heterostructured quantum dots, Adv. Mater. **26**, 8034 (2014).
[39] A. Thoma, P. Schnauber, M. Gschrey, M. Seifried, J. Wolters, J.-H. Schulze, A. Strittmatter, S. Rodt, A. Carmele, A. Knorr *et al.*, Exploring dephasing of a solid-state quantum emitter via time-and temperature-dependent Hong-Ou-Mandel experiments, Phys. Rev. Lett. **116**, 033601 (2016).
[40] M. Shim and P. Guyot-Sionnest, Permanent dipole moment and charges in colloidal semiconductor quantum dots, J. Chem. Phys. **111**, 6955 (1999).
[41] S. A. Empedocles and M. G. Bawendi, Quantum-confined Stark effect in single CdSe nanocrystallite quantum dots, Science **278**, 2114 (1997).
[42] S. Aghaeimeibodi, C.-M. Lee, M. A. Buyukkaya, C. J. Richardson, and E. Waks, Large Stark tuning of InAs/InP quantum dots, Appl. Phys. Lett. **114**, 071105 (2019).
[43] A. L. Efros, M. Rosen, M. Kuno, M. Nirmal, D. J. Norris, and M. Bawendi, Band-edge exciton in quantum dots of semiconductors with a degenerate valence band: Dark and bright exciton states, Phys. Rev. B **54**, 4843 (1996).
[44] P. C. Sercel and A. L. Efros, Band-edge exciton in CdSe and other II–VI and III–V compound semiconductor nanocrystals- revisited, Nano Lett. **18**, 4061 (2018).
[45] A. L. Efros and A. L. Efros, Interband absorption of light in a semiconductor sphere, Sov. Phys. Semicond. **16**, 772 (1982).
[46] A. I. Ekimov, F. Hache, M. Schanne-Klein, D. Ricard, C. Flytzanis, I. Kudryavtsev, T. Yazeva, A. Rodina, and A. L. Efros, Absorption and intensity-dependent photoluminescence measurements on CdSe quantum dots: Assignment of the first electronic transitions, J. Opt. Soc. Am. B **10**, 100 (1993).
[47] T. D. Krauss and L. E. Brus, Charge, polarizability, and photoionization of single semiconductor nanocrystals, Phys. Rev. Lett. **83**, 4840 (1999).